Fern-like rGO/$BiVO_4$ hybrid nanostructures for high-energy symmetric supercapacitor

Santosh S. Patil[‡,a,c] *Deepak P. Dubal*[‡,b] *Virendrakumar G. Deonikar*[a] *Mohaseen S. Tamboli,*[a] *Jalindar D. Ambekar,*[a] *Pedro Gomez-Romero,*[b,*] *Sanjay S. Kolekar,*[c] *Bharat B. Kale,*[a,*] *Deepak R. Patil*[a,*]

[a]*Centre for Materials for Electronics Technology, Department of Electronics and Information Technology (DeitY), Govt. of India. Pune*

[b]
Catalan Institute of Nanoscience and Nanotechnology (ICN2), CSIC and The Barcelona Institute of Science and Technology, Campus UAB,
Bellaterra, 08193 Barcelona, Spain

[c]*Analytical Chemistry and Material Science Laboratory, Dept. of Chem., Shivaji University, Kolhapur, India*

‡These authors contributed equally

***Corresponding Author Emails**

deepphys24@gmail.com, bbkale@cmet.gov.in, pedro.gomez@cin2.es

Abstract

Herein, we demonstrate synthesis of rGO/$BiVO_4$ hybrid nanostructures by a template-free hydrothermal method. Morphological studies reveal that rGO sheets are embedded in the special dendritic fern-like structures of $BiVO_4$. The hybrid architectures formed show the way to a rational design of supercapacitor, since these structures enable easy access of electrolyte ions by reducing internal resistance. Considering the unique advantages of morphological features of rGO/$BiVO_4$ hybrid nanostructures, they were used as electrode materials for supercapacitor application. The rGO/$BiVO_4$ electrode showed a specific capacitance of 151 F/g at a current density of 0.15 mA/cm^2 with a wide potential window between -1.0 to 0.6 V (Vs Ag/AgCl) higher than the traditional carbon-based cells. Furthermore, we demonstrated rational design of a rGO/$BiVO_4$ based symmetric capacitor which provides an extended voltage window of 1.6 V and leads to an excellent energy density of 1.6 mWh/cm^3 (33.7 Wh/ kg) and ensures rapid energy delivery with power density of 391 mW/cm^3 (8.0 kW/Kg). The superior properties of symmetric supercapacitor can be attributed to the special dendritic fern-like $BiVO_4$ morphology and intriguing physicochemical properties of rGO.

Keywords: rGO/$BiVO_4$, Fern/dendritic structures, High energy density, Symmetric supercapacitor

1. Introduction

Nowadays, the use of fossil fuels for energy has become a serious societal concern due to environment pollution, global warming, and rapid resource depletion.[1,2] Therefore, finding sustainable and cost-effective energy conversion and energy storage devices is urgently needed in order to meet the increasing energy demand of society.[3] Among different energy storage systems, supercapacitors have attracted intense research attention from the scientific community due to their excellent performance at high power rates.[4] Supercapacitors store electrical energy through charge accumulation on electrode-electrolyte interface (Electric double layer capacitors) or Faradaic redox reaction (Pseudocapacitors). Metal oxides (binary or tertiary),[5] metal sulphides,[6] two-dimensional (2D) layered materials including graphene,[7] reduced graphene oxide,[8] and their composites[9] have been exemplified as high-performance supercapacitor electrodes. However, the low energy density (<10 Wh/kg) of these supercapacitors has remained a major challenge in employing them as primary power sources to replace batteries.[10] Therefore, increasing energy density of supercapacitor is of prime importance in order to employ them for large scale practical applications.

Two most commonly used strategies for increasing the energy density of supercapacitors are the design of high-voltage supercapacitors with wider potential windows and developing hybrid (asymmetric) supercapacitors with one capacitive electrode and other faradaic electrode.[10] Currently, research in this field is mostly focused on asymmetric capacitors which use pseudo-capacitive or faradaic material as positive and EDLC carbon as negative electrodes in aqueous electrolytes. Although asymmetric supercapacitors present high energy densities and cycling stabilities, the energy density and specific capacitances of carbon anodes are still insufficient to counter balance the electrochemical performance of positive electrode materials. Moreover, asymmetric supercapacitors involve a complex balancing of charges from the different electrochemistries in negative and positive electrodes. On the other hand, construction of symmetric supercapacitors is an effective approach to solve this problem, however; this

requires strict criteria on the electrodes and electrolytes to give high operation voltage and high-level capacitance with good rate capability.

There are very few transition metal oxide (TMOs) materials such as RuO_2,[11] $Co(OH)_2$,[12] MnO_2,[13] VO_2[14] and NiO[15] have been reported for symmetric supercapacitor application which exhibited high voltage window and excellent supercapacitor performance. Among them, vanadium (IV) oxide (VO_2) based symmetric supercapacitors showed better electrochemical performance with high energy density, power density and cycling stability.[14] Most recently, $BiVO_4$ (belonging to the vanadate family) has been reported as one of the novel anode material for asymmetric supercapacitor application.[16] Owing to excellent physicochemical properties and stability, $BiVO_4$ has also been used previously for gas sensing, ferroelasticity and photocatalysis applications.[16,17] However, previous studies have proven that $BiVO_4$ possesses relatively poor electronic conductivity which hampers rate capability and capacitance retention because of the low charge transfer rate in fast charging and discharging process. Therefore, electronic conductivity of $BiVO_4$ needs to be improved. One of the most promising approaches to improve the electronic conductivity of $BiVO_4$ is to prepare hybrid composites by integrating $BiVO_4$ with carbon based materials.[4,18] It is well-known that carbon-based materials show excellent electrical conductivity and can serve as a buffer layer to compromise the volume change of $BiVO_4$.[19] Among the various carbon analogs, reduced graphene oxide (rGO) represents good electrical conductivity, chemical stability and high surface area which can suppress the volume change and particle agglomeration during the charge-discharge process.[20] In addition, rGO also facilitates the penetration of aqueous electrolyte and introduces pseudocapacitive effects.[21] Thus, the synergic combination of rGO with $BiVO_4$ would have several advantages due to distinctive features of rGO and could represent a rational design of hybrid material for high performance supercapacitor device.

In this respect, innovative rGO/$BiVO_4$ hybrid architectures were prepared by a facile hydrothermal method. These rGO/$BiVO_4$ hybrid nanostructures did undergo different physical-chemical characterizations such as structural, compositional and morphological etc. Later, the electrochemical performance of rGO/$BiVO_4$ hybrid material was tested by fabricating symmetrical supercapacitors with

KOH electrolyte. Certainly, the rGO/$BiVO_4$ based symmetric cell allows for the realization of a broad voltage of 1.6 V in aqueous electrolyte. This value is well beyond the thermodynamic stability window of water (1.23 V), and remarkably comparable to asymmetric systems. The combination of additional conductivity of rGO in $BiVO_4$ and widened voltage window of this really synergic electrode material allows for attaining a remarkable energy density of 1.6 mWh/cm^3.

2. Experimental

Commercial graphite (Sigma-Aldrich) was used as source to prepare reduced graphene oxide. Sodium nitrate ($NaNO_3$, 99%; Fisher Scientific), potassium permanganate ($KMnO_4$, 99%; SDFCL), and hydrogen peroxide (H_2O_2, 30%; Fisher Scientific), Hydrochloric acid (HCl, 38%; SDFCL), Sulphuric acid (H_2SO_4,98%; SDFCL), Bismuth (III) nitrate ($Bi(NO_3)_3.5H_2O$, 98.5%; SDFCL), Ammonium metavanadate (NH_4VO_4, 99%; Fisher Scientific) (Qualigen Chemicals Limited), , Ammonia (NH_3, 25%; Qualigen Chemicals Limited) and Nitric acid (HNO_3, 71%; Fisher Scientific), were also used as starting materials. All the chemicals were of AR grade and used without any further purification.

2.1 Synthesis of graphene oxide (GO)

Graphene oxide (GO) was prepared by modified Hummers method[22] through exfoliation of a chemically oxidized flake graphite powder. For the synthesis of GO, 1 g of graphite was added into concentrated H_2SO_4 (23 mL) in a round-bottom flask and stirred on magnetic stirrer under an ice bath. Then, 3 g of $KMnO_4$ were gradually added under intensive stirring under cooled condition and maintained at 20 ^oC for 10 minutes. Further, the mixture was kept at 35 °C and magnetically stirred for 4 h to achieve a dark brown color paste. After this, 46 mL of distilled water was added into the mixture to increase the temperature to 98 ^oC and maintained for 15 minutes. Subsequently, 140 mL of distilled water was added followed by addition of 10 ml 30% H_2O_2 solution. The mixture was subjected to centrifugation and washed 3-4 times with 5% HCl solution. The obtained GO product was dried and used for further reaction. The GO powder was annealed at 800 ^oC under N_2 atmosphere to achieve the reduced graphene oxide (rGO) nanosheets.

2.2 Synthesis of rGO/$BiVO_4$ hybrid nanostructures

The synthesis of rGO/$BiVO_4$ hybrid nanostructures was carried out by facile hydrothermal method. In a detailed synthesis, a mixed solvent was prepared by using 65 ml distilled H_2O and 5 ml HNO_3 solution. To the as prepared solvent, the rGO powder (1 mg/ml) was put and ultrasonicated for 2h in order to exfoliate rGO. Then, solvent is divided into two portions of 35 ml. Then, 5 mmol of Bi $(NO_3)_3.5H_2O$ was dissolved in 35 ml of solvent. Similarly, 5 mmol of NH_4VO_4 were dissolved separately 35 ml of solvent. Subsequently, NH_4VO_4 solutions was added drop wise to the solution of Bi $(NO_3)_3.5H_2O$ at room temperature under vigorous magnetic stirring and maintained pH around 7 by addition of NH_3. Finally the entire solution was transferred into Teflon reactor and kept at 180 ^oC for 24 hours. After reaction the reactor was allowed to cool naturally to room temperature. The precipitate was collected and washed thoroughly with distilled water and ethanol, dried at 60 ^oC for 3 h and used for further characterization. For comparison pristine $BiVO_4$ powder was also prepared under similar reaction conditions.

2.3 Materials Characterization:

The phase analysis of the samples were performed by X-ray diffraction (XRD) on a Rigaku-Ultima III with CuKα radiation (λ = 1.5418 Å. The X-ray photoelectron spectra (XPS) analyses were obtained by X-ray photoelectron spectroscopy (XPS, SPECS Germany, PHOIBOS 150). The surface morphology of as-prepared samples were investigated using the field-emission scanning electron microscopy (FEI Quanta 650F Environmental SEM) attached with an energy-dispersive X-ray spectroscopy (EDS) analyzer to measure the sample composition.

2.4 Electrochemical measurements

To check the electrochemical performances of synthesized materials, the working electrodes were prepared by using Doctor Blade method. For this, 85 % of active material (rGO/$BiVO_4$) was mixed with 10 % PVDF as binder and 5 % acetylene black. A few drops of N-Methyl-2-pyrrolidone (NMP, solvent) were added and the mixture was homogenized using a mortar to get a uniform paste. Finally, the paste was applied on commercial flexible carbon cloth which was further used as SCs electrodes. The resultant

thin films were then annealed at 180 ^{o}C for two hours in order to remove the binder. The typical mass loading of the electrode material was around 0.5-0.9 mg/cm^2. The electrochemical properties were measured using standard three electrode system which contains working electrodes ($BiVO_4$ and $rGO/BiVO_4$), counter electrode (platinum) and reference electrode (Ag/AgCl) in 6 M KOH electrolyte. Symmetric cell was constructed in a 3-way Teflon Swagelok cell using two identical electrodes of $rGO/BiVO_4$ with polypropylene separator sandwiched between them and few drops of 6 M KOH electrolyte. Two channels from potentiostat were connected together in such a way that one channel records voltage between two electrodes (positive and negative) and other channel records potential contributed from positive and negative electrodes with respect to reference electrode. All electrochemical measurements (cyclic voltammetry (CV) and galvanostatic charge-discharge (CD) techniques) were carried out using a Biologic VMP3 potentiostat.

3. Results and discussion:

Figure 1a compares the X-Ray diffraction (XRD) patterns of as-prepared $BiVO_4$ and $rGO/BiVO_4$ nanostructures. XRD patterns confirm the formation of crystalline monoclinic phase of $BiVO_4$ with lattice constants a = 0.5185 nm, b = 1.1713 nm and c = 0.5102 nm which are in good agreement with literature values (JCPDS card no 014-0688). In the case of $rGO/BiVO_4$ nanostructures no characteristic diffraction peaks for rGO were observed which might be due to the weak diffraction intensities of rGO compared to those of $BiVO_4$ or due to the low content of graphene oxide employed in the reaction.

Further, elemental surface composition analysis was determined by X-Ray photoelectron spectroscopy. Figure 1b-d depicts the XPS spectra of $rGO/BiVO_4$ hybrid nanostructures which confirm the presence of C, Bi, V and O elements. The existence of Carbon peaks is mainly due to the presence of rGO in rGO/ $BiVO_4$ hybrid nanostructures. The core level XPS signal of C 1s (Figure 1b) exhibited a main peak centered at about 284.6 eV originated from the graphitic sp2 carbon atoms and two weak peaks located at 286.6 eV (C−O, epoxy, and hydroxyl) and 288.9 eV (C=O, carboxyl) were due to oxygen containing functional groups.[23] The moderately low peak intensity of oxygenated functional groups

indicates efficient removal of oxygen-containing functional groups during the hydrothermal process. The spin orbit component of Bi 4f peak are deconvoluted into two curves with binding energies of Bi $4f_{7/2}$ (159.0 eV) and Bi $4f_{7/2}$ (165 eV) (Figure 1c). Similarly, the split peaks for V2p were observed at binding energy 524.2 eV and 516.7 eV that corresponds to V $2p_{1/2}$ and V $2p_{3/2}$ orbital's respectively. The XPS spectrum of O1s showed asymmetric behavior which indicates existence of different oxygen species on the surface. The peak located at 529.9 eV is attributed to lattice oxygen of $BiVO_4$ (Figure 1d)[24, 25] and another deconvoluted O 1s peak at 531.6 eV is ascribed to surface hydroxyl groups.[25]

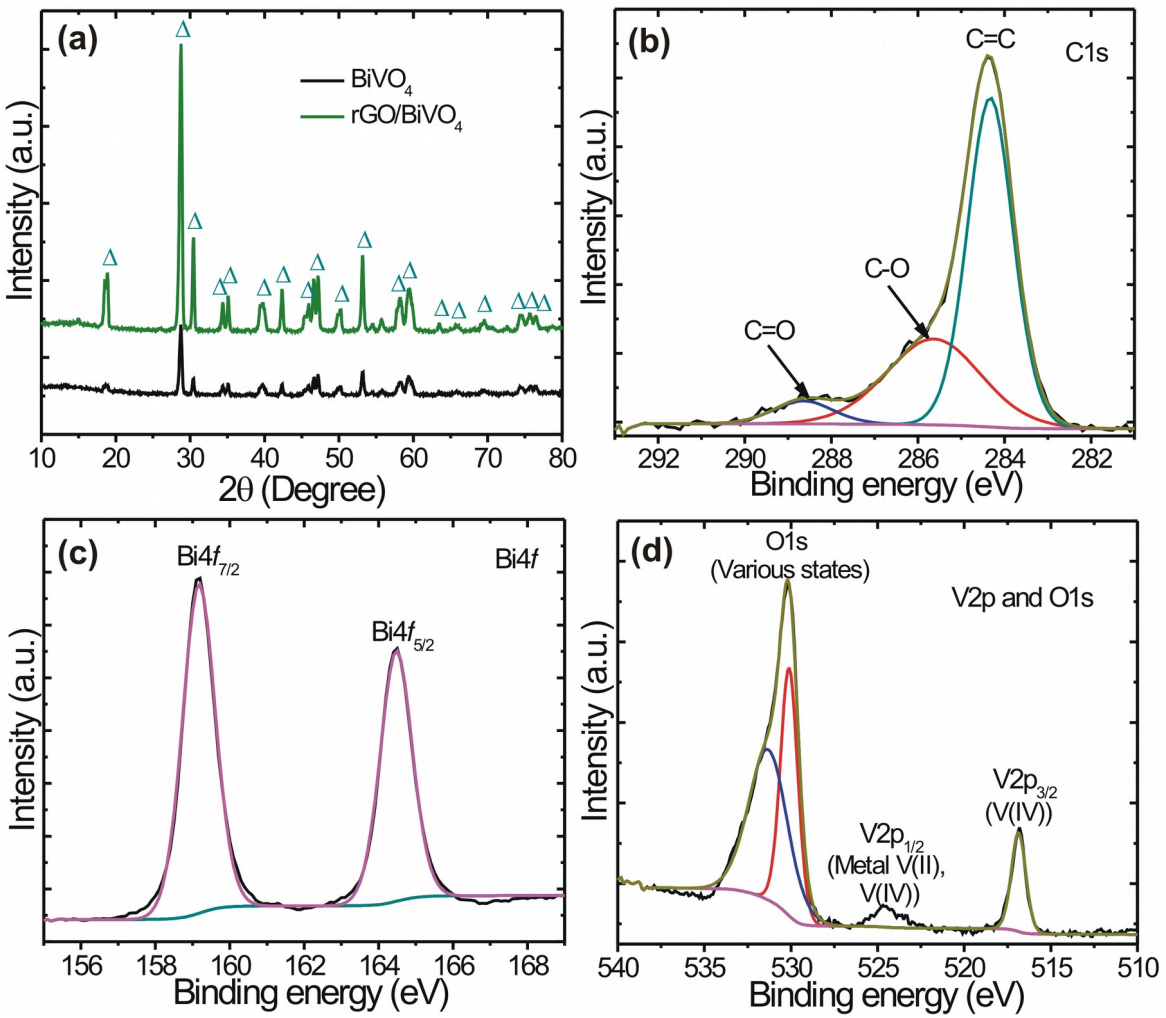

Figure 1 (a) XRD patterns of $BiVO_4$ and rGO/$BiVO_4$ (b) XPS spectra of C 1s (c) XPS spectra of Bi 4f and (d) XPS spectra of V 2p and O 1s

Morphological features of as-prepared $BiVO_4$ and rGO/$BiVO_4$ samples were investigated by FESEM (Figure 2a-f) technique. A special dendritic fern-like morphology was observed for $BiVO_4$ (see, Figure 2a) which has gained a renowned research interest due to the remarkable connectivity between the crystals, that enables the construction of high performance supercapacitor electrodes.[26,27] Importantly, dendrite consists of a number of branches densely packed together which can afford high porosity favoring facile access of the electrolyte ions.[26] Figures 2a and b clearly evidence the typical dendrite fern-like morphology for $BiVO_4$ which is formed by number of branches with length size in 200-500 nm. The average length of intact single fern structure is found to be around 4–5 μm which is supported by unique backbone. During hydrothermal reaction, due to rotation of particles via Brownian motion or short-range interaction between the particles, branches (rod like structures) are formed which act as building blocks for fern development. The growth of these branches takes place via Ostwald ripening and always tries to adjust structures to achieve a minimum total surface free energy.[28] It should be noted that an isotropic growth of branches along [001] direction is responsible for formation of special $BiVO_4$ dendrite structures.[29]

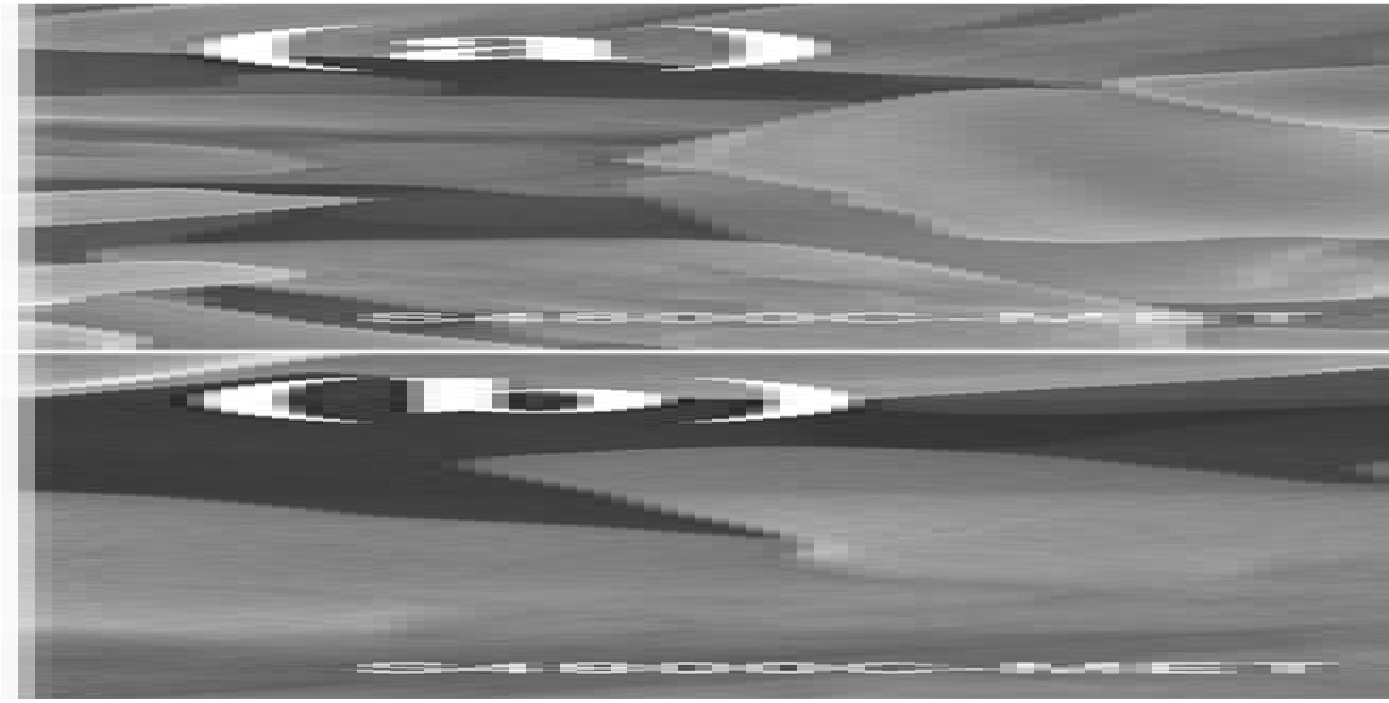

Figure 2 FESEM micrographs of (a, b) $BiVO_4$ and (c-f) rGO/$BiVO_4$ hybrid nanostructure

A close look at FESEM images (Figure 2b-d) clearly revealed that the rGO sheets (thickness around 100 nm) were embedded into the $BiVO_4$ dendrite structures. In particular, rGO helps to enhance the conductivity of the hybrid material as well as it also facilitates fast transportation of electrons during electrochemical reaction. It was previously assumed that the rGO nanosheets can greatly reduce the diffusion length over which both ions and electrons must transfer during the charge-discharge process. Owing to unique dendrite morphology of $BiVO_4$ and appropriate rGO (high surface area material) combination, rGO/$BiVO_4$ hybrid nanostructures could bear better electrochemical performance for supercapacitor.

Furthermore, the electrochemical properties of the $BiVO_4$ and rGO/$BiVO_4$ hybrids were investigated in two electrode swagelok cells in 6 M KOH electrolyte by using cyclic voltammetry (CV) and charge-discharge (CD) cycling. Figure 3a depicts the CV curves of $BiVO_4$ and rGO/$BiVO_4$ electrodes at various scan rates exhibiting a wide potential window from -1.0 to 0.6 V. The deviation in a CV curve from ideal rectangular shape indicates pseudo-capacitive behavior of $BiVO_4$ and rGO/$BiVO_4$ electrodes. Two pairs of redox current peaks were observed for rGO/$BiVO_4$ electrode corresponding to the redox pairs Bi(II)/Bi(III) and V(IV)/V(V), which were distinguishable from those of electric double-layer capacitors, indicating the presence of a faradaic reaction. It should be noted that such feature was not observed for $BiVO_4$ electrode, where only one redox peak is observed. This might be due to strong chemical interaction between the $BiVO_4$ dendrites and the residual oxygen containing functional groups on the RGO or van der Waals interactions between them.[30] Furthermore, as the scan rate increases the area under the curve increases retaining redox peaks even at high scan rates suggesting excellent rate capability of this material. The galvanostatic charge/discharge (GCD) curves of $BiVO_4$ (Figure 3c) and rGO/$BiVO_4$ (Figure 3d) electrodes were recorded at different current densities which showed that the rGO/$BiVO_4$ hybrid electrode has a longer discharge time, signifying relatively higher specific capacitance. This might be due to relatively good electrical conductivity of rGO/$BiVO_4$ hybrid

architecture contributed from rGO, thereby facilitate the electron transfer during the charge/discharge process.

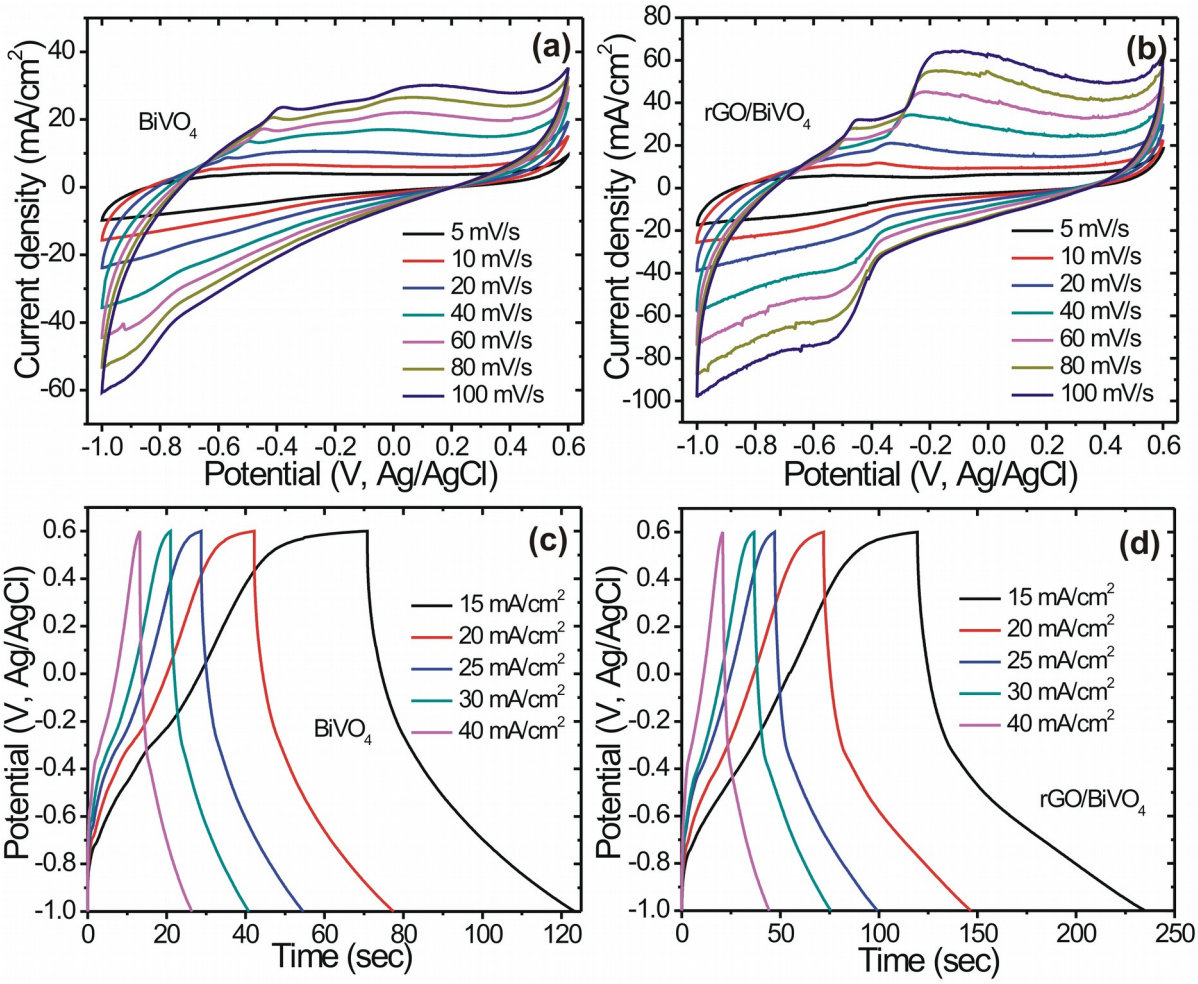

Figure 3 Cyclic voltammetry (CV) curves of (a) $BiVO_4$ and (b) $rGO/BiVO_4$ electrodes at different scanning rates and Galvanostatic charge/discharge (CD) curves of (c) $BiVO_4$ and (d) $rGO/BiVO_4$ electrodes at different current densities.

Figure 4 summarizes the effect of incorporation of rGO into $BiVO_4$ on the electrochemical performances. Figure 4a compares the CV curves for the $BiVO_4$ and $rGO/BiVO_4$ electrodes at constant scan rate of 40 mV/s. It is noteworthy that although there is no significant change in operational voltage window, the current density of $rGO/BiVO_4$ hybrid electrode was increased drastically compared to that of pure $BiVO_4$ electrode.

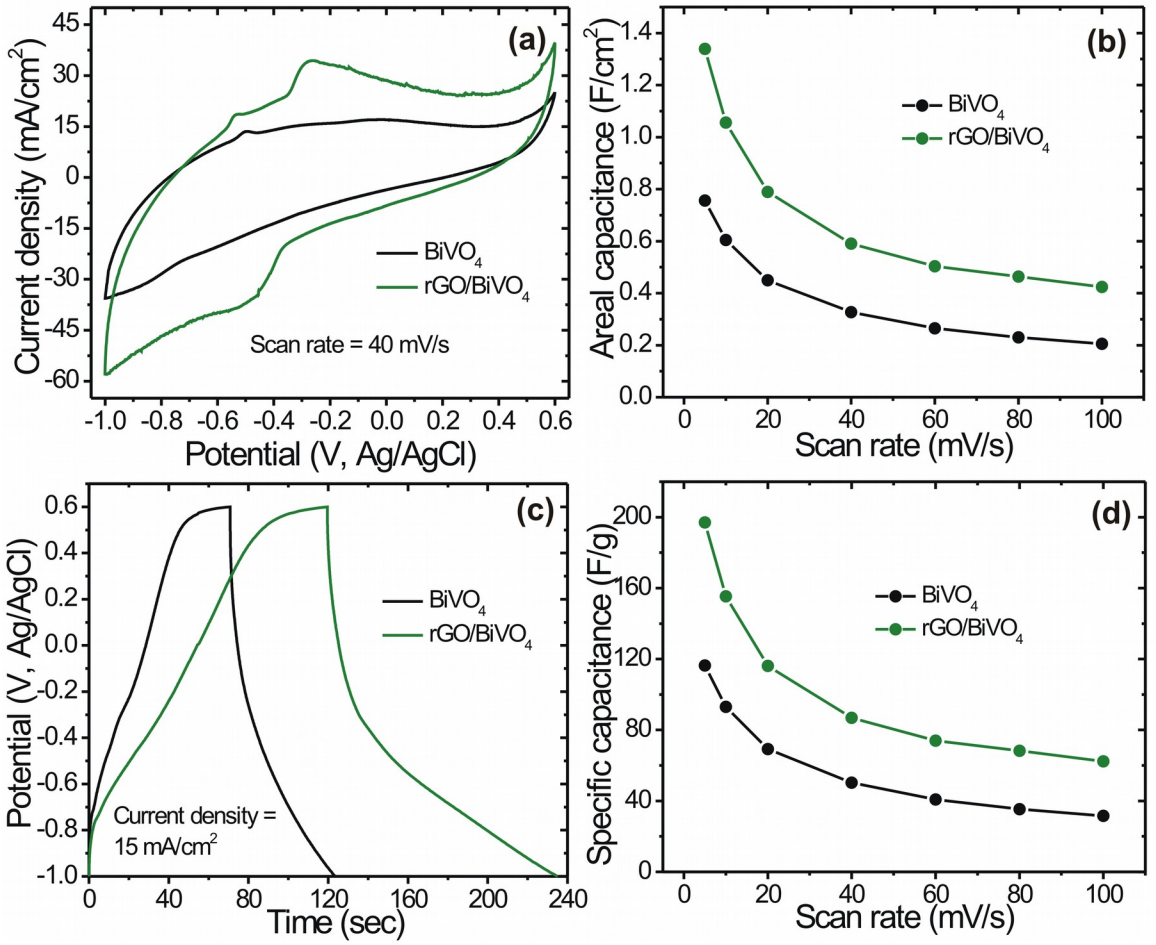

Figure 4 (a) Cyclic voltammetry curves of $BiVO_4$ and $rGO/BiVO_4$ electrodes at constant scan rate of 40 mV/s and (b) Variation of Areal capacitance of $BiVO_4$ and $rGO/BiVO_4$ electrodes as a function of scan rates (c) chronopotentiometry curves of $BiVO_4$ and $rGO/BiVO_4$ electrodes at current density of 15 mA/cm^2 (d) Variation of specific capacitance of $BiVO_4$ and $rGO/BiVO_4$ electrodes as a function of scan rates.

Similarly, Figure 4c indicates the comparison of the discharge curves at 15 mA/cm^2 for $BiVO_4$ and $rGO/BiVO_4$ electrodes. The hybrid $rGO/BiVO_4$ based electrode showed substantially longer (almost double) discharge time than that of the pure $BiVO_4$ sample, indicating a significantly larger specific capacitance. For the quantitative analysis of the electrochemical performance, the specific capacitances were derived from the CV measurements (supporting information S.I. 1). Figure 4b and d shows the

variation of areal and specific capacitance of $BiVO_4$ and rGO/$BiVO_4$ electrode at different scan rates, respectively. The maximum areal (specific) capacitances obtained for $BiVO_4$ and rGO/$BiVO_4$ electrodes are 0.75 F/cm^2 (116.3 F/g) and 1.33 F/cm^2 (196 F/g) respectively, at a scan rate of 5 mV/s. The rGO/$BiVO_4$ electrode shows enhanced electrochemical performance than that of BiVO4. This shows that rGO have a significant influence on electrochemical activity of $BiVO_4$ in the hybrid nanostructure. Pure $BiVO_4$ exhibits an inferior rate capability as compared with the rGO/$BiVO_4$ electrodes. There are several factors endow the superior electrochemical performance of rGO/$BiVO_4$ hybrid nanostructures. First, the controlled assembly of dendritic $BiVO_4$ structures which enables easy access of electrolyte ions by reducing internal resistance and electronically conducting graphene nanosheets. Second, the intimate interfacial interaction between the graphene sheets and the $BiVO_4$ matrix provides electron superhighways, allowing for rapid and efficient charge transport and leading to an increase in the overall electronic conductivity.[30]

Since the rGO/$BiVO_4$ hybrid electrode can work within a wider potential window from -1.0 to 0.6 V (*vs* Ag/AgCl) and can show superiority for electrochemical charge storage, we assembled a symmetric cell based on rGO/$BiVO_4$ electrodes by sandwiching KOH-soaked separator in between. In present case, the rGO/$BiVO_4$ electrode can be used a positive as well as negative electrode for supercapacitor application. The electrochemical properties of symmetric cell were evaluated by CV, CD, cyclic stability and impedance measurements. Figure 5a shows cyclic polarization curves of rGO/$BiVO_4$//rGO/$BiVO_4$ symmetric cell at various scanning rates. Interestingly, the symmetric cell exhibit high potential window (1.6 V) beyond thermodynamic limit of water (1.23 V). In addition, as evident from the CV curves, a fabricated symmetric cell retains rectangular shape even at high scan rates suggesting good rate capability of electrode materials. Furthermore, as seen from Figure 4b, the acquired galvanostatic CD curves for rGO/$BiVO_4$ symmetric cell at various current densities ranging from 1.42 A/g to 10.0 A/g showed longer discharge time, indicating high rate capability of cell.

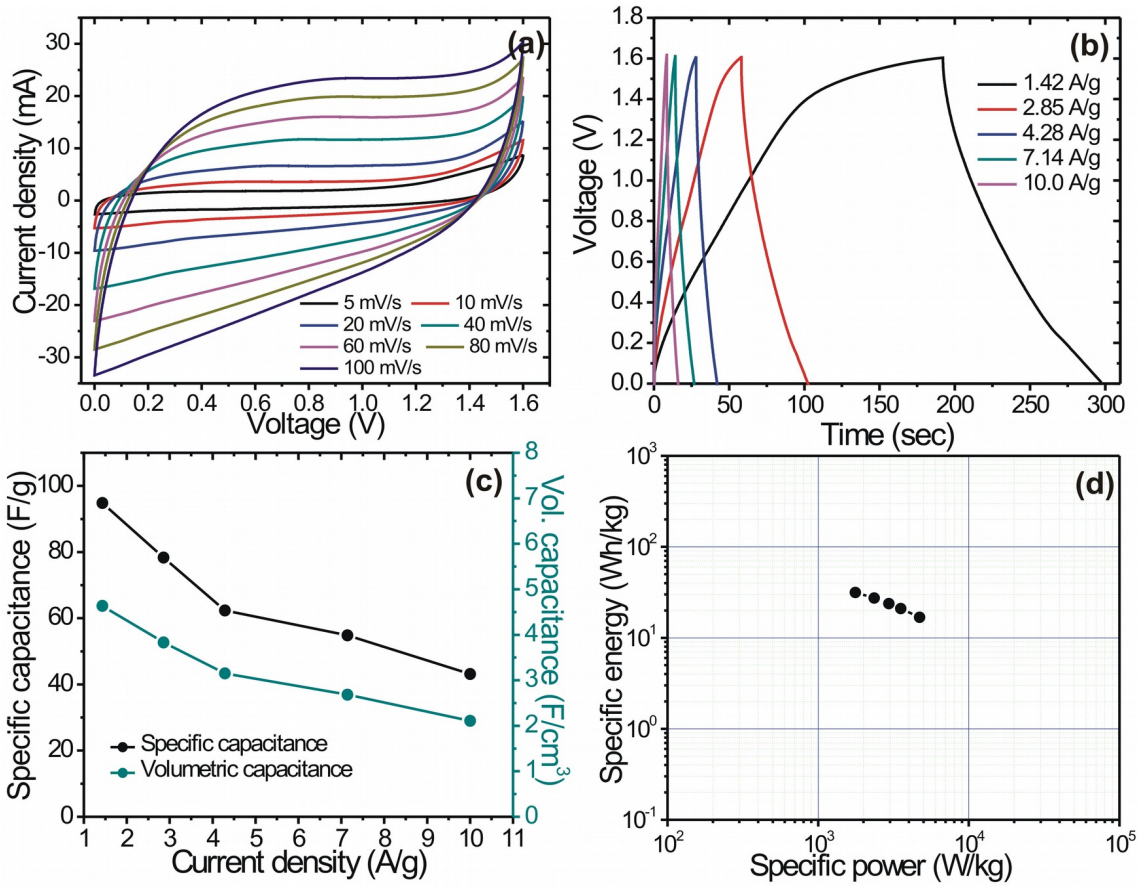

Figure 5 (a) CV curves of rGO/$BiVO_4$ based symmetric cell at different scanning rates, (b) Galvanostatic charge/discharge (CD) curves of rGO/$BiVO_4$ based symmetric cell at different current densities (c) Variation of specific capacitance and volumetric capacitance of rGO/$BiVO_4$ symmetric cell at different current densities (d) Gravimetric energy/power densities of rGO/$BiVO_4$ symmetric cell

The specific and volumetric capacitances of symmetric cell at different current densities were calculated (supporting information S. I. 1) and plotted in Figure 5c. The rGO/$BiVO_4$ symmetric cell provides a high volumetric capacitance of 4.63 F/cm^3 (94.83 F/g for total mass of both electrodes 4.9 mg/cm^2) at a current density of 1.40 A/g. There is gradual reduction in capacitance up to 2.10 F/cm^3 (43 F/g) was observed with increasing current density because of diffusion limitation caused by ionic motion of electrolyte. The gravimetric/volumetric energy density and power density of rGO/$BiVO_4$ symmetric cell were calculated from CD curves and shown as a Ragone plot in Figure 5d and 6 a. The maximum

volumetric energy density of cell is found to be 1.63 mWh/cm^3 (33.7 Wh/kg) at power density of 55 mW/cm^3 (1.14 kW/kg). It is noteworthy that, even at high power density of 391 mW/cm^3 (8.00 kW/kg), rGO/$BiVO_4$ symmetric cell still exhibits energy density of 0.75 mWh/cm^3 (15.33 Wh/kg), thereby, confirms their potential for application in high performance devices. These values of volumetric energy density are considerably higher than those of previous reports on symmetric and asymmetric supercapacitors with aqueous electrolyte such as H-TiO_2@MnO_2 //H-TiO_2@C (0.30 mWh/cm^3, 5M LiCl),[31] Co_9S_8//Co_3O_4@RuO_2 (1.21 mWh/cm^3, 3M KOH),[32], VOx//VN (0.61 mWh/cm^3, 5M LiCl),[33] MnO_2//MnO_2 (0.023 mWh/cm^3, polyvinylpyrrolidone (PVP)-6 M $LiClO_4$ gel electrolyte)[13] laser-scribed graphene (LSG)//LSG (0.09 mWh/cm^3, 1 M H_3PO_4)[34], RGO//RGO (0.0031 mWh/cm^3 2M H_2SO_4),[35] RGO–RuO_2//RGO–RuO_2 (0.012 mWh/cm^3 2M H_2SO_4),[35] RGO–PANi//RGO–PANi (0.013 mWh/cm^3, 2M H_2SO_4)[35] The high energy and power densities of the rGO/$BiVO_4$ symmetric cell is a result of high voltage window (1.6 V) and improved electrical conductivity due to rGO incorporation into $BiVO_4$ dendritic nanostructures.

Cycling stability is one of the most important features of high-performance supercapacitor devices and determines their application in industry. Our rGO/$BiVO_4$ symmetric cell was subjected to 2000 galvanostatic charging discharging cycles at a current density of 4 A/g and the capacitance retention of the cell is plotted in Figure 6b. It was observed that the rGO/$BiVO_4$ symmetric cell retains 80.3 % of its specific capacitance up to 2000 cycles, indicating good capacitance retention which is higher than those of earlier reported systems composed of $BiVO_4$ asymmetric capacitor (42% after 200 cycles)[16] and VO_2// VO_2 based symmetric supercapacitor (78.7 % after 4500 cycles).[14] It is important to note that, previously Shivakumara *et al.*[36] have demonstrated 86% capacitance retention for rGO//rGO symmetric cell after 3000 charge discharge cycles however, the energy density and power density values of the same are lower compared to our rGO/$BiVO_4$//rGO/$BiVO_4$ symmetric cell.

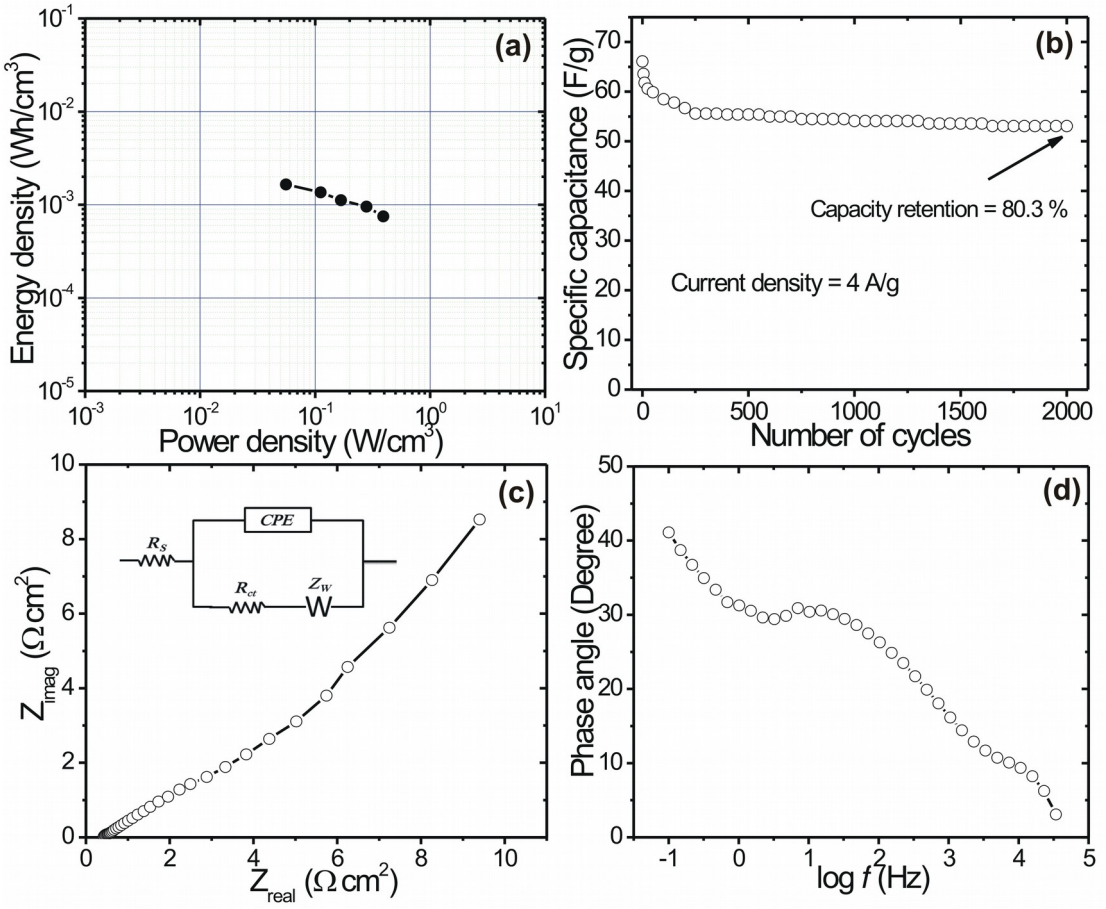

Figure 6 (a) volumetric energy/power densities of rGO/$BiVO_4$ symmetric cell (b) Cycle performance of rGO/$BiVO_4$ symmetric cell at current density of 4 A/g, (c) Nyquist plots of rGO/$BiVO_4$ symmetric cell after 2000 cycles, (d) Plot of phase angle with frequency rGO/$BiVO_4$ symmetric cell.

Impedance spectra were recorded in order to investigate the bulk solution resistance (R_e), charge transfer resistance (R_{ct}), and Warburg resistance (Z_w) of as synthesized electrode materials. Figure 6d depicts the Nyquist plots of the rGO/$BiVO_4$ symmetric cell and inset shows equivalent circuit for the Nyquist plot. Nyquist plot showed a very low ESR value (0.5 Ω) which demonstrates that rGO/$BiVO_4$ has a very small internal resistance with a good ion response in high frequency ranges. For a more informative analysis, the dependence of phase angle with frequency of the symmetric cell was plotted in

Figure 7d. The phase angle of 40° with broad capacitive region signifies a high capacitive character with enhanced charge transfer due to the favorable electrode/electrolyte interface.[37]

From the above discussion, it becomes obvious that our rGO/$BiVO_4$ hybrid system for symmetric supercapacitor exhibits better electrochemical supercapacitive properties which could be assigned to combined effect of rGO and $BiVO_4$ nanostructures. The present work highlights assembling of symmetric cells which could eliminate the use of complex chemistries usually involved in asymmetric cells (different electrode materials) as well as complication in balancing the charge (or mass) of both electrodes. Therefore, the rGO/$BiVO_4$ symmetric cell shows the way to a rational design for the development of the high-voltage asymmetric counterparts under the same power in order to achieve high energy/power density for supercapacitors.

Conclusion

In summary, a facile, cost-effective and template-free hydrothermal method has been successfully employed for the synthesis of rGO/$BiVO_4$ hybrid fern/dendrite structures. A symmetric cell based on rGO/$BiVO_4$ hybrid electrode has been successfully fabricated representing excellent supercapacitive properties. Most specifically, the rGO/$BiVO_4$ based symmetric cell offers an extended voltage window of 1.6 V leading to an excellent energy density of 1.60 mWh/cm^3 (33.7 Wh/kg) with a high power density of 391 mW/cm^3 (8.0 kW/Kg). Moreover, our symmetric cell exhibits a significantly high volumetric capacitance of 4.63 F/cm accompanied by improved cycling stability (80% retention after 2000 cycles), which makes it an efficient candidate in the field of supercapacitors.

Acknowledgement:

Authors wish to thanks Nanocrystalline materials and Glass laboratory, C-MET Pune for their characterization support. Authors would like to thank Department of Science and Technology (DST) INSPIRE faculty program and Department of Electronics and Information Technology (DeitY, New

Delhi) for financial support. DPD and PGR acknowledge partial support from the Spanish Miisterio MINECO (Grant MAT2015-68394-R,MINECO/FEDER) and appreciate the award with the support of the Secretary for Universities and Research of the Ministry of Economy and Knowledge of the Government of Catalonia and the Co-fund programme of the Marie Curie Actions of the 7th R&D Framework Programme of the European Union. DPD and PGR also acknowledge AGAUR (Generalitat de Catalunya) for Project NESTOR (Nanomaterials for Energy STORage) 2014_SGR_1505

References

(1) Yu, G.; Xie, X.; Pan, L.; Bao, Z.; Cui, Y. Hybrid Nanostructured Materials for High-Performance Electrochemical Capacitors. *Nano Energy* **2013**, *2*, 213–234.

(2) Dubal, D. P.; Ayyad, O.; Ruiz, V.; Gómez-Romero, P. Hybrid Energy Storage: The Merging of Battery and Supercapacitor Chemistries. *Chem. Soc. Rev.* **2015**, *44*, 1777–1790.

(3) Peng, X.; Peng, L.; Wu, C.; Y, X. Two Dimensional Nanomaterials for Flexible Supercapacitors. *Chem. Soc. Rev.* **2014**, *43*, 3303–3323.

(4) Dubal, D. P.; Holze, R.; Gomez-Romero, P. Development of Hybrid Materials Based on Sponge Supported Reduced Graphene Oxide and Transition Metal Hydroxides for Hybrid Energy Storage Devices. *Sci. Rep.* **2014**, *4*, 7349-7359.

(5) Lokhande, C. D.; Dubal, D. P.; Joo, O. S. Metal oxide thin film based supercapacitors. *Curr Appl. Phys.* **2011**, 11, 255-270

(6) Ratha, S.; Rout, C. S. Supercapacitor Electrodes Based on Layered Tungsten Disulfide-Reduced Graphene Oxide Hybrids Synthesized by a Facile Hydrothermal Method. *ACS Appl. Mater. Interfaces* **2013**, *5*, 11427–11433.

(7) Lei, Z.; Shi, F.; Lu, L. Incorporation of MnO_2-Coated Carbon Nanotubes between Graphene Sheets as Supercapacitor Electrode. *ACS Appl. Mater. Interfaces* **2012**, *4*, 1058–1064.

(8) Sahu, V.; Shekhar, S.; Sharma, R. K.; Singh, G. Ultrahigh Performance Supercapacitor from Lacey Reduced Graphene Oxide Nanoribbons. *ACS Appl. Mater. Interfaces* **2015**, *7*, 3110–3116.

(9) Zhang, Z.; Wang, Q.; Zhao, C.; Min, S.; Qian, X. One-Step Hydrothermal Synthesis of 3D Petal-like Co_9S_8 /RGO/Ni_3S_2 Composite on Nickel Foam for High-Performance Supercapacitors *ACS Appl. Mater. Interfaces* **2015**, *7*, 4861–4868.

(10) Gao, H.; Xiao, F.; Ching, C. B.; Duan, H. High-Performance Asymmetric Supercapacitor Based on Graphene Hydrogel and Nanostructured MnO_2. *ACS Appl. Mater. Interfaces* **2012**, *4*, 2801–2810.

(11) Xia, H.; Meng, S.; Yuan, G.; Cui, C.; Lu, L. A Symmetric RuO_2/RuO_2 Supercapacitor Operating at 1 . 6 V by Using a Neutral Aqueous Electrolyte. *Electrochem. Solid-State Lett.* **2012**, *15*, 60–63.

(12) Jagadale, A. D.; Kumbhar, V. S.; Dhawale, D. S.; Lokhande, C. D. Electrochimica Acta Performance Evaluation of Symmetric Supercapacitor Based on Cobalt Hydroxide [Co($OH)_2$] Thin Film Electrodes. *Electrochim. Acta* **2013**, *98*, 32–38.

(13) Chodankar, N. R.; Dubal, D. P.; Gund, G. S.; Lokhande, C. D.; Chodankar, N. R.; Dubal, D. P.; Gund, G. S.; Lokhande, C. D. A Symmetric MnO_2/ MnO_2 Flexible Solid State Supercapacitor Operating at 1.6 V with Aqueous Gel Electrolyte. *J. Energy Chem.* **2016,** *25*,463-471.

(14) Ma, X-J.; Zhang W-B.; Kong L-B.; Luo,Y.-C.; Kang, L. VO_2: From Negative Electrode Materials to Symmetric Electrochemical Capacitors. *RSC Adv.* **2015**, *5*, 97239–97247.

(15) Ganesh, V.; Pitchumani, S.; Lakshminarayanan, V. New Symmetric and Asymmetric Supercapacitors Based on High Surface Area Porous Nickel and Activated Carbon. *J. Power Sources* **2006**, *158*, 1523–1532.

(16) Khan, Z.; Bhattu S.; Haram, S.; Khushalani, D.; SWCNT/$BiVO_4$ Composites as Anode Material for Supercapacitor Application *RSC Adv.* **2014**, *4*, 17378–17381.

(17) Zhao, Y.; Xie, Y.; Zhu, X.; Yan, S.; Wang, S. Surfactant-Free Synthesis of Hyperbranched Monoclinic Bismuth Vanadate Batteries. *Chem. Eur. J.* **2008**, *14*, 1601–1606.

(18) Chen, H.; Zhou, S.; Wu, L. Porous Nickel Hydroxide-Manganese Dioxide-Reduced Graphene Oxide Ternary Hybrid Spheres as Excellent Supercapacitor Electrode Materials. *ACS Appl. Mater. Interfaces* **2014**, 6 (11), 8621-8630.

(19) Xu, L.; Chen, H.; Shu, K. $Ni(OH)_2$/RGO Nanosheets Constituted 3D Structure for High-Performance Supercapacitors. *J. Sol-Gel Sci. Technol.* **2015**,*77*, 463-469.

(20) Ma, H.; He, J.; Xiong, D.; Wu, J.; Li, Q.; Dravid, V.; Zhao, Y. Nickel Cobalt Hydroxides @ Reduced Graphene Oxide Hybrid Nanolayers for High Performance Asymmetric Supercapacitors with Remarkable Cycling Stability *ACS Appl. Mater. Interfaces* **2016, 8(3)**, 1992-2000.

(21) Chen, Y.; Zhang, X.; Zhang, D.; Yu, P.; Ma, Y. High Performance Supercapacitors Based on Reduced Graphene Oxide in Aqueous and Ionic Liquid Electrolytes. *Carbon*, **2011**, 4*9*, 573-580.

(22) Hummers, W. S.; Offema, R. E. Preparation of Graphitic Oxide. *J. Am. Chem. Soc.* **1957**, *208*, 1937.

(23) Seo, M.; Yoon, D.; Seon, K.; Won, J.; Kim, J. Supercritical Alcohols as Solvents and Reducing Agents for the Synthesis of Reduced Graphene Oxide. *Carbon* **2013**, 6*4*, 207-218.

(24) Liu, S.; Yin, K.; Ren, W.; Cheng, B.; Yu, J. Tandem Photocatalytic Oxidation of Rhodamine B over Surface Fluorinated Bismuth Vanadate Crystals. *J. Mater. Chem.* **2012**, *22*, 17759–17767.

(25) Ge, L. Novel Pd /$BiVO_4$ Composite Photocatalysts for Efficient Degradation of Methyl Orange under Visible Light Irradiation. *Mater. Chem. Phys.* **2008**, *107*, 465–470.

(26) Sun, Z.; Firdoz, S.; Yap, Esther Y-X.; Li, L.; E.; Lu, X. Hierarchically Structured MnO_2 Nanowires Supported on Hollow Ni Dendrites for High-Performance. *Nanoscale* **2013**, *5*, 4379–4387.

(27) Zou, R.; Zhang, Z.; Yuen, M. F.; Hu, J.; Lee, C.; Zhang, W. Dendritic Heterojunction Nanowire Arrays for High-Performance Supercapacitors. *Sci. Rep.* **2015**, *5*, 1–7.

(28) Panmand, R. P.; Patil, R. H.; Kale B. B.; Nikam, L. K.; Kulkarni, M. V.; Thombre, D. K.; Gade W. N.; Gosavi, S. W. Self Assembly of Nanostructured Hexagonal Cobalt Dendrites: An Efficient Anti-Coliform Agent. *RSC. Adv.* **2014**, *4*, 4586–4595.

(29) Zhou, L.; Wang, W.; Xu, H. Mesocrystals via a Facile Additive-Free Aqueous Strategy & Design, *Cryst. Growth Des.* **2008**, *8*, 728–733.

(30) Wang, H-W.; Hu, Z-A.; Chang, Y-Q.; Chen, Y-L.; Wu, H-Y.; Zhang, Z. Y.; Yang, Y. Y. Design and Synthesis of $NiCo_2O_4$–reduced Graphene Oxide Composites for High Performance Supercapacitors. *J. Mater. Chem. A* **2011**, *21*, 10504–10511.

(31) Lu, X.; Yu, M.; Wang, G.; Zhai, T.; Xie, S.; Ling, Y. H-TiO_2 @ MnO_2//H-TiO_2@C Core – Shell Nanowires for High Performance and Flexible Asymmetric Supercapacitors. *Adv. Mater.* **2013**, *25*, 267–272.

(32) Xu, J.; Wang, Q.; Wang, X.; Xiang, Q.; Liang, B.; Chen, D.; Shen, G. Flexible Asymmetric Supercapacitors Based upon Co_9S_8 Nanorod//Co_3O_4@RuO_2 Nanosheet Arrays on Carbon Cloth. *ACS Nano* **2013**, *7*, 5453–5462.

(33) Lu, X.; Yu, M.; Zhai, T.; Wang, G.; Xie, S.; Liu, T.; Liang, C.; Tong, Y.; Li, Y. High Energy Density Asymmetric Quasi-Solid-State Supercapacitor Based on Porous Vanadium Nitride Nanowire Anode. *Nano Lett.* **2013**, *13*, 2628–2633.

(34) El-kady, M. F.; Srong, V.; Dubin, S.; Kaner, R. B. Laser Scribing of High-Performance and Flexible Graphene-Based Electrochemical Capacitors. *Science* **2012**, *335*, 1326–1330.

(35) Zhang, J.; Jiang, J, Li, H.; Zhao, X. S. A High-Performance Asymmetric Supercapacitor Fabricated with Graphene-Based Electrodes. *Energy Environ. Sci.* **2011**, *4*, 4009–4015.

(36) Shivakumara, S.; Kishore, B.; Tirupathi Rao P.; Munichandraiah. N. Symmetric Supercapacitor Based on Reduced Graphene Oxide in Non-Aqueous Electrolyte *ECS Electrochem. Lett.* **2015**, *4*, 87–89.

(37) Ujjain, S. K.; Ahuja, P.; Sharma, R. K. Graphene Nanoribbon Wrapped Cobalt Manganite Nanocubes for High Performance All-Solid-State Fl Exible Supercapacitors. *J. Mater. Chem. A* **2015**, *3*, 9925–9931.